

Effect of long-range random potentials on the electronic transport properties of disordered semiconductors: A numerical study

H. Overhof and M. Schmidtke

Fachbereich Physik, Universität-GH Paderborn, D-33098 Paderborn, Germany

(Received 8 October 1999)

A numerical model is used to calculate dc conductivity, thermoelectric power, and Hall mobility of quasi-classical carriers subject to a long-range static random potential. The convergence of the results with respect to the model parameters is investigated. The long-range spatial coherence of the random potential is shown to affect the results to some degree, but less than inferred from the earlier study.

I. INTRODUCTION

The concept of a long-range random potential that modulates the mobility edges of amorphous semiconductors has been introduced by Tauc¹ in 1970 and by Fritzsche² in 1971 in order to explain the discrepancy between optical and electrical band gaps in these systems. This concept was further used to explain a variety of phenomena, as e.g., the difference between the activation energies of the electrical dc conductivity and of the thermoelectric power,³⁻⁵ the change of the drift mobility upon doping⁶ in singly doped *a*-Si:H, the broadening of the optical tail in compensated *a*-Si:H,⁷ and many other phenomena, see e.g., Ref. 8. In compensated crystals and in doped amorphous semiconductors a random potential is caused by the nonhomogeneity of a random distribution of charged dopants,⁹⁻¹¹ but other effects can also contribute, as e.g., hydrogenated dangling bonds¹² and structural inhomogeneities.^{13,14}

In this paper we study (as in Ref. 4) electronic transport by nondegenerate electrons above a mobility edge, modulated by a random static potential with a characteristic wavelength that exceeds both the elastic and the inelastic scattering length. In a semiclassical description the random potential modulates the local carrier density and therewith the local conductivity. At elevated temperatures, the electronic current is nonzero in the entire sample with some preference to regions with low values of the random potential. As the temperature is lowered, the regions that effectively carry the current will shrink to filaments with cross sections that tend to zero. The highest potential on such a filament determines the activation energy of the dc conductivity while the thermoelectric power, connected with the mean energy transported by the electronic current, provides a measure of the mean potential on this filament. Hence the activation energy of the dc conductivity is expected to exceed the activation energy of the thermoelectric power by some quantity E_Q^* , which is observed experimentally in *a*-Si:H (Ref. 3) and other amorphous semiconductors (see Ref. 5).

While also many other experimental results have been interpreted in terms of a random potential, little is known about the correlation of the amplitude of the random potential or rather its variance δ with experimental data like E_Q^* . To date, only the earlier numerical study by one of the present authors⁴ has addressed the three-dimensional (3D)

transport problem. The limited computing power available at the time caused a restriction to very small model sizes. It was concluded that for a given value of δ the value obtained for E_Q^* depends sensitively on the correlation of the random potential. Recently this conclusion has been challenged by 2D model calculations.¹⁴ In the present paper we reinvestigate the problem to find out whether the discrepancy between the two papers is caused by the different dimensionalities. Furthermore, we make use of the computer power available today to investigate the numerical reliability of the results.

II. NUMERICAL MODEL

We consider cubic samples of length $N \cdot L$ that are divided into $N \times N \times N$ subcubes of length L ($N \times N$ subsquares for 2D systems). L must be larger than the elastic and the inelastic scattering lengths, but much smaller than the characteristic wavelength of the random potential. It is then possible to approximate $V(\vec{r})$ in subcube i by its average value $V(i)$, assigning a local conductivity $\sigma_i(T)$ to subcube i

$$\sigma_i(T) = \sigma_0 \exp\left(-\frac{E_C - E_F + V(i)}{k_B T}\right). \quad (1)$$

In a second step the sample is replaced by an equivalent network of conductors. From the resulting current distribution we obtain the local current densities $\vec{j}(\vec{r})$ and the averaged sample conductivity σ and compare it with the conductivity σ_0 of a sample with $\delta=0$.

From the current density the heat current transported by the electrical current of carriers with charge q

$$\vec{w}_q(\vec{r}) = \frac{1}{q} \vec{j}(\vec{r}) [E_C - E_F + V(\vec{r}) + A k_B T] \quad (2)$$

is calculated using a constant heat of transport term $A \approx 1$. From $\vec{w}_q(\vec{r})$ we calculate the mean Peltier coefficient Π and Π_0 , the Peltier coefficient for $\delta=0$, from which the contribution of the random potential to the thermoelectric power is obtained

$$\hat{S} = \frac{1}{q} \frac{\Pi - \Pi_0}{T}. \quad (3)$$

Combining conductivity and thermoelectric power we obtain

$$\hat{Q}(T) = \overline{\ln(\sigma/\sigma_0)} + \frac{q}{k_B} \bar{\delta}(T), \quad (4)$$

where the overline indicates a configurational average (see below).

The Hall effect is calculated from the longitudinal current densities, assigning local transverse Hall fields within the subcubes. In a second step the network equations for the transverse Hall voltages are solved. We thus obtain the averaged Hall mobility μ_H in terms of μ_0 , the Hall mobility for $\delta=0$. It is essential to decouple the calculation of the transverse Hall voltages from the much larger longitudinal voltages. Even with this precaution, the calculation of the Hall mobility for lower temperatures is subject to numerical inaccuracies.

In order to avoid the computer-time consuming construction of the random potential from the Coulomb potential of screened point charges (as in Ref. 4) we start in this paper with a Gaussian potential distribution of variance δ . Assigning random values to the subcubes results in a random potential V_{start} without spatial correlation. A potential with a finite correlation length is obtained from V_{start} averaging each potential $V(i)$ with the potential of the 26 adjacent subcubes (8 subsquare in 2D cases). The procedure is repeated n_{av} times and results in a potential with a Gaussian distribution and a correlation length $l_{\text{cor}} \approx 1.7 \sqrt{n_{\text{av}}} L$.

For infinite systems a single sample (i.e., a single random potential data set) would determine the transport parameters. In a numerical treatment restricted to finite systems we have performed configurational averages, since different samples lead to somewhat different transport parameters. The results presented in this study are always configurationally averaged over 100 sample, a number that proved sufficient for the determination of mean values and variances ε .

A fair representation of $V(\vec{r})$ by a steplike potential $V(i)$ requires N to be large. While the numerical effort to solve a conductance network problem consisting of N^3 nodes is greatly reduced because the conductance matrix is sparse, the computational effort still rises proportional to N .⁷ For 2D systems our calculations are limited to $N \leq 100$, while for 3D systems the limit is $N \leq 45$. This in turn means that for 3D systems neither $L \ll l_{\text{cor}}$ nor $l_{\text{cor}} \ll N \cdot L$ can really be fulfilled. We shall show, however, that our results, within certain limitations, are representative for infinite systems. In order to reduce the effect of the surfaces of our finite samples, we use periodic boundary conditions in transverse direction, a precaution that for $N \geq 20$ turned out not to be necessary.

A. Convergence with respect to sample size

Since the conductivity Eq. (1) depends exponentially on the potentials $V(i)$, a configurational average should start from $\ln(\sigma/\sigma_0)$ rather than from σ/σ_0 . In Fig. 1 we therefore plot the mean value $\overline{\ln(\sigma/\sigma_0)}$ for 3D samples of different size N . Since the spread becomes important for larger values of $\delta/k_B T$, we show results for $\delta/k_B T = 10$, the lowest temperature considered in this study. The distribution function of the individual values of $\ln(\sigma/\sigma_0)$ closely resembles a Gaussian of width $\varepsilon[\ln(\sigma/\sigma_0)]$, which is also indicated in Fig. 1.

Also shown in Fig. 1 are averaged values for the sample conductances and the sample resistances, respectively. The

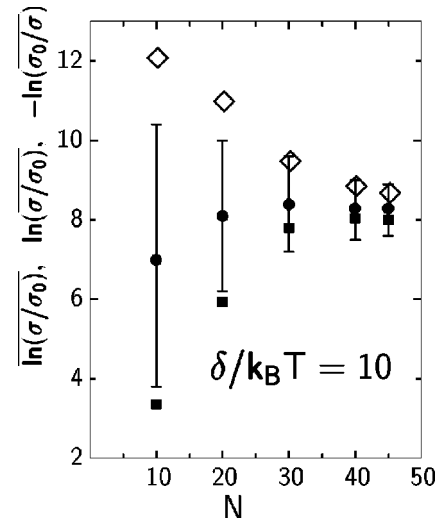


FIG. 1. $\overline{\ln(\sigma/\sigma_0)}$ (full spheres), $\overline{\ln(\sigma_0/\sigma)}$ (empty diamonds), and $-\overline{\ln(\sigma_0/\sigma)}$ (squares) for the $N \times N \times N$ resistor model with $z=6$ and $\delta/k_B T = 10$ as a function of N . The bars denote the variance $\varepsilon[\ln(\sigma/\sigma_0)]$.

former value is dominated by the samples with the highest conductances, while the latter is dominated by samples with the largest resistivity value. For $N \leq 20$ both the distributions of σ/σ_0 and σ_0/σ turn out to be very asymmetric, and the rare occurrence of samples with exceptionally large values virtually prohibited the determination of converged averages σ/σ_0 and σ_0/σ , respectively.

While for $N=10$, the conductances of individual samples vary by five orders of magnitude, Fig. 1 shows that for $N \geq 30$ the spread is greatly reduced. While the differences between $\overline{\ln(\sigma/\sigma_0)}$, $\overline{\ln(\sigma_0/\sigma)}$, and $-\overline{\ln(\sigma_0/\sigma)}$ are reduced with rising N , the averaged values $\overline{\ln(\sigma/\sigma_0)}$ are practically identical for $N \geq 20$, indicating convergence with respect to the sample size.

B. Analogous percolation problem

In the limit $\delta/k_B T \gg 1$, the conductance problem for uncorrelated random potentials can be approximated, dividing the subcubes into two classes, conducting subcubes with $V(i) \leq V_c$ and nonconducting subcubes with $V(i) \geq V_c$ in analogy to open and blocked sites of a site percolation problem.¹⁵ A “critical concentration” p_c (depending on the geometry of the network) of sites must be open in order to have the first contiguous “critical path” of open sites extend through the sample.

The equivalent to the critical path is a path with $V(i) \leq V_c$ in all subcubes. In the low-temperature limit this path carries the total current. From the analogy, V_c can be determined via

$$p_c = \int_{-\infty}^{V_c} p(V) dV, \quad (5)$$

which is also the low-temperature activation energy E_σ of the network conductance. In a similar manner the average Peltier heat can be approximated by

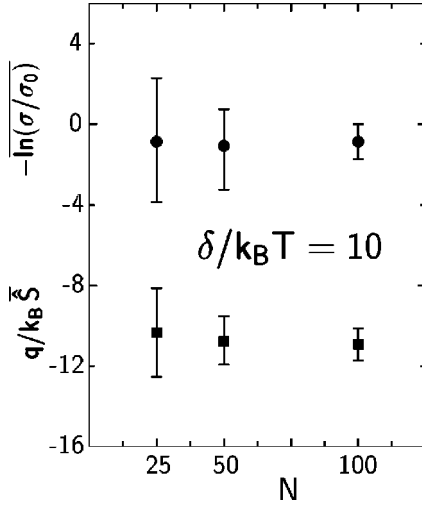


FIG. 2. $\overline{\ln(\sigma/\sigma_0)}$ (full spheres) and $q/k_B \bar{S}$ (full squares) for the two-dimensional $N \times N$ resistor model with $z=4$ and $\delta/k_B T=10$ as a function of N . The bars denote the variances $\varepsilon[\ln(\sigma/\sigma_0)]$ and $\varepsilon(q/k_B \bar{S})$, respectively.

$$E_{\Pi} = \frac{1}{p_c} \int_{-\infty}^{V_c} V \cdot p(V) dV. \quad (6)$$

III. RESULTS

In this section we discuss the results obtained both for 2D and 3D systems. The results for 2D systems are of particular interest, because comparison can be made with recent model calculations of Quicker and Kakalios.¹⁴

A. 2D systems

Results for 2D models with $n_{av}=3$ are shown in Fig. 2. Clearly, the results are converged with respect to N . If we approximate

$$\hat{Q}(T) = \hat{Q}_0 - \frac{E_Q^*}{k_B T} \quad (7)$$

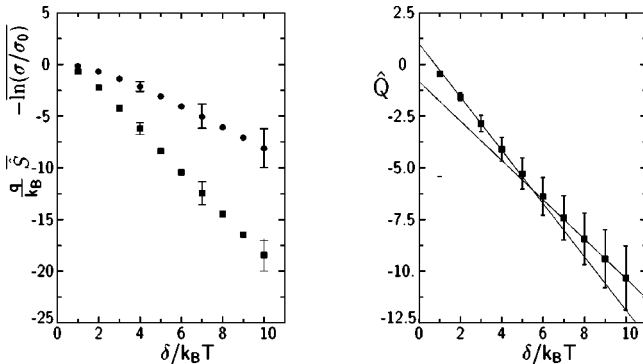


FIG. 3. $\overline{\ln(\sigma/\sigma_0)}$ (spheres) compared with $q/k_B \bar{S}$ (squares) (left) and \hat{Q} (right) calculated for a $20 \times 20 \times 20$ resistor network model as a function of the normalized inverse temperature for $z=6$. The bars denote the variances of the individual values.

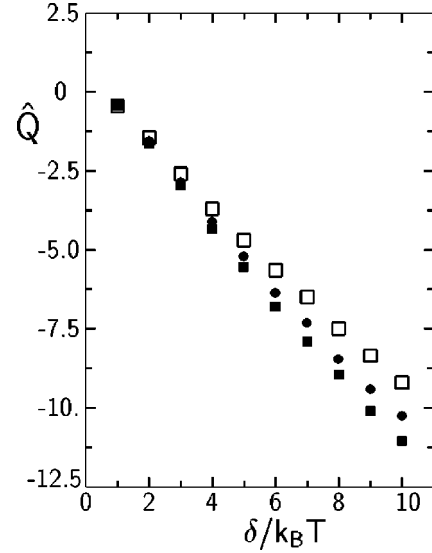


FIG. 4. \hat{Q} is plotted vs $\delta/k_B T$, for $10 \times 10 \times 10$ samples (open squares), for $20 \times 20 \times 20$ samples (full circles), and for $40 \times 40 \times 40$ samples (full squares).

we obtain $E_Q^* \sim 1.16\delta$. We observe that for 2D systems the results are rather independent of n_{av} , in agreement with Quicker and Kakalios.¹⁴

B. 3D systems

The transport data for a 3D network with $N=20$ are plotted in Fig. 3. $q/k_B \bar{S}$ appears to be activated with $E_S^* = 2.0\delta$. As in the 2D case, σ/σ_0 rises with rising $\delta/k_B T$, because the highest value of the potential encountered on the current-carrying path is negative, an effect that is much more pronounced in a 3D system ($p_c=0.307$ for a 3D, $z=6$ cubic lattice¹⁵) than in a 2D system (with $p_c=0.59$ for a $z=4$ 2D square network).

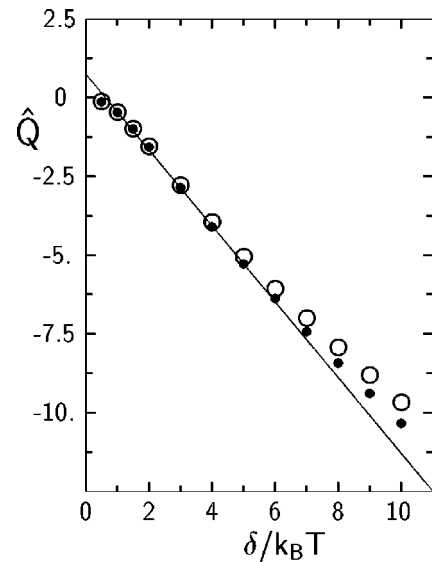


FIG. 5. \hat{Q} calculated for 100 $20 \times 20 \times 20$ systems plotted vs $\delta/k_B T$ (full spheres) are compared with calculations (open spheres) where the random potential has been coarse-grained blocks of eight subcubes. An extrapolation for the high-temperature limits is also indicated.

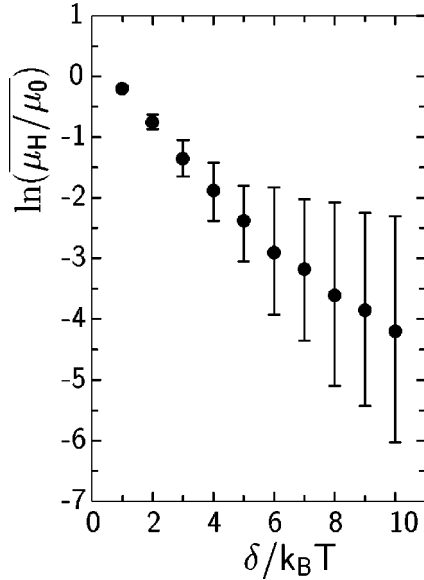


FIG. 6. $\ln(\mu_H/\mu_0)$ and $\varepsilon[\ln(\mu_H/\mu_0)]$ plotted vs $\delta/k_B T$ for $20 \times 20 \times 20$ samples.

The results for σ/σ_0 displayed in Fig. 3 show larger deviations from a strictly activated behavior and, therefore, \hat{Q} also exhibits a distinct kink near $\delta/k_B T \approx 5$. Figure 4 shows this kink not to be an effect of the sample size: with rising N , the kink is shifted to somewhat larger values of $\delta/k_B T$, but apparently does not disappear.

Instead this kink is caused by the finite size of the subcubes: As discussed above, the cross section of the current-carrying path is reduced until it approaches a single line in the zero-temperature limit. In contrast, in our numerical model the size of the subcube sets a strict lower limit to all cross sections, giving rise to the kink observed in \hat{Q} .

In Fig. 5 results for \hat{Q} for two different sets of $N=20$ samples are compared to illustrate this effect. The first set is standard calculation with $n_{av}=3$. In the second set, the potential of the first set was coarse grained, replacing the potential of blocks of $2 \times 2 \times 2$ subcubes by its average value. As is clearly seen, coarse-grained potentials lead to a kink at higher temperatures when compared with results from potential without coarse graining.

IV. HALL EFFECT

Although the sign of the Hall effect in amorphous semiconductors has been known to be anomalous for more than 20 years,³ this sign anomaly is still not understood to date. Clearly, it is not just a consequence of disorder, since the anomaly is absent in microcrystalline samples¹⁶ and disappears in recrystallized amorphous samples.¹⁷ Our model calculations are performed assuming a normal Hall effect in the absence of a random potential.

In Fig. 6 we show the effect of the random potential on the Hall mobility for this case. For $\delta/k_B T \leq 5$ the Hall mobility is activated with a well-defined activation energy E_H . For larger values of $\delta/k_B T$ the slope of the Hall mobility

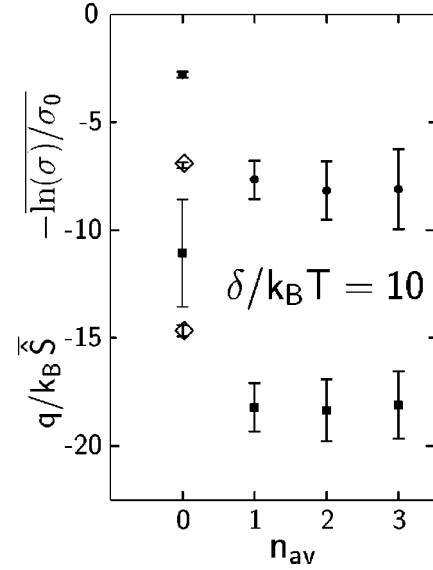


FIG. 7. $-\ln(\sigma/\sigma_0)$ (spheres) compared with $q/k_B \bar{S}$ (squares) for a $20 \times 20 \times 20$ resistor model with $z=6$ at $\delta/k_B T=10$ as a function of n_{av} . For $n_{av}=0$ the results for $z=18$ are shown as open diamonds.

gradually decreases, whereas the variance ε of the Hall mobility increases. Since a calculation of μ_H is plagued with the same cross-section problem of the current-carrying path as the dc conductivity, we have not been able to determine the low-temperature value of μ_H any further and note that a well-defined activation energy is observed only for the smaller values of $\delta/k_B T$.

V. DISCUSSION

In a previous paper⁴ it had been claimed that the slope $E_{\hat{Q}}^*$ of \hat{Q} is small compared to δ unless the potential is long range with $l_{cor} \gg L$. This claim has been challenged recently.¹⁴ Results obtained for a 2D model with uncorrelated potentials lead to a slope $E_{\hat{Q}}^*$ that is about 2/3 of the slope derived from potentials with $l_{cor} \gg L$. We have checked this result for 2D systems and obtain similar numbers. For 3D systems the difference between results for \hat{Q} derived from correlated and from uncorrelated potentials is similar to 2D systems. In Fig. 7 we show results for $\ln(\sigma/\sigma_0)$ and for $q/k_B \bar{S}$ obtained for 3D samples at $\delta/k_B T=10$ with different values of n_{av} . The value of \hat{Q} increases by about 30% when going from $n_{av}=0$ to $n_{av}=1$, with marginal changes for larger values of n_{av} . Also shown in Fig. 7 are results for $n_{av}=0$ for a model with $z=18$. Obviously a change of the coordination number affects the conductivity and the thermoelectric power data leading to rather minor changes for \hat{Q} only.

From our present result, the best estimate for the transport parameters in the presence of a random potential can be summarized as

$$\ln(\sigma/\sigma_0) = -0.6 + 0.82 \frac{\delta}{k_B T}, \quad (8)$$

$$\frac{q}{k_B} S = 1.6 - 2.1 \frac{\delta}{k_B T}, \quad (9)$$

$$\hat{Q} = 1.0 - 1.28 \frac{\delta}{k_B T}, \quad (10)$$

$$\ln(\mu_H/\mu_0) = 0.07 - 0.5 \frac{\delta}{k_B T} \quad (11)$$

in reasonable agreement with the previous results⁴ ($\hat{Q} = 1.8 - 1.75\delta/k_B T$) obtained for 3D samples of size $10 \times 10 \times 10$, for which the convergence was questionable.

In contrast to the earlier results⁴ the results presented here can be considered as well converged with respect to the sample size, at least for $\delta/k_B T \lesssim 5$. Furthermore, in general agreement with Ref. 14, we find a sizable slope E_Q for uncorrelated potentials as well. If these have a Gaussian distribution, we obtain a value of E_Q that is about 2/3 of the value given in Eq. (10) for the correlated random potential.

¹J. Tauc, Mater. Res. Bull. **5**, 721 (1970).

²H. Fritzsche, J. Non-Cryst. Solids **6**, 49 (1971).

³W. Beyer, H. Mell, and H. Overhof, in *Amorphous and Liquid Semiconductors*, edited by W.E. Spear (CICL, Edinburgh, 1977), p. 328; W. Beyer and H. Mell, *ibid.*, p. 333.

⁴H. Overhof and W. Beyer, Philos. Mag. B **44**, 317 (1981).

⁵H. Overhof and P. Thomas, *Electronic Transport in Hydrogenated Amorphous Semiconductors*, Springer Tracts in Modern Physics. Vol. 114 (Springer, Berlin, 1989).

⁶R.A. Street, J. Kakalios, and M. Hack, Phys. Rev. B **38**, 5608 (1988).

⁷J.A. Howard and R.A. Street, Phys. Rev. B **44**, 7935 (1991).

⁸H. Overhof, Solid State Phenom. **44-46**, 535 (1995).

⁹B.I. Shklovskii and A.L. Efros, Fiz. Tekh. Poluprovodn. **4**, 305

(1970) [Sov. Phys. Semicond. **4**, 247 (1970)]; Zh. Éksp. Teor. Fiz. **60**, 867 (1971) [Sov. Phys. JETP **33**, 468 (1971)]; **62**, 1156 (1972) [**35**, 610 (1972)].

¹⁰B.I. Shklovskii and A.L. Efros, *Electronic Properties of Doped Semiconductors*, Springer Series in Solid-State Sciences Vol. 45 (Springer, Berlin, 1984).

¹¹J. Jäckle, Philos. Mag. B **41**, 681 (1980).

¹²B. Kramer, H. King, and A. MacKinnon, J. Non-Cryst. Solids **59-60**, 73 (1983).

¹³H. Fritzsche, Thin Solid Films **90**, 119 (1982).

¹⁴D. Quicker and J. Kakalios, Phys. Rev. B **60**, 2449 (1999).

¹⁵V.K.S. Shante and S. Kirkpatrick, Adv. Phys. **20**, 325 (1971).

¹⁶W.E. Spear, G. Willeke, P.G. LeComber, and A.G. Fitzgerald, J. Phys. **4**, 247 (1981).

¹⁷O.J. Reilly and W.E. Spear, Philos. Mag. B **38**, 295 (1978).